Song, M., Renson, L., Noël, J. P., Moaveni, B., & Kerschen, G. (2018). Bayesian model updating of nonlinear systems using nonlinear normal modes. *Structural Control and Health Monitoring*, *25*(12), [e2258]. https://doi.org/10.1002/stc.2258

Bayesian Model Updating of Nonlinear Systems using Nonlinear Normal Modes

Mingming Song[1], Ludovic Renson[2], Jean-Philippe Noël[3], Babak Moaveni[1], and Gaetan Kerschen[3]

[1]*Dept. of Civil and Environmental Engineering, Tufts University, Medford, MA, USA*
[2]*Dept. of Engineering Mathematics, University of Bristol, Bristol, UK*
[3]*Dept. of Aerospace and Mechanical Engineering, University of Liege, Liege, Belgium*

Abstract

This paper presents a Bayesian model updating methodology for dynamical systems with geometric nonlinearities based on their nonlinear normal modes (NNMs) extracted from broadband vibration data. Model parameters are calibrated by minimizing selected metrics between identified and model-predicted NNMs. In a first approach, a deterministic formulation is adopted, and parameters are updated by minimizing a nonlinear least-squares objective function. A probabilistic approach based on Bayesian inference is next investigated, where a Transitional Markov Chain Monte Carlo is implemented to sample the joint posterior probability distribution of the nonlinear model parameters. Bayesian model calibration has the advantage to quantify parameter uncertainty and to provide an estimation of model evidence for model class selection. The two formulations are evaluated when applied to a numerical cantilever beam with geometrical nonlinearity. The NNMs of the beam are derived from simulated broadband data through nonlinear subspace identification and numerical continuation. Accuracy of model updating results is studied with respect to the level of measurement noise, the number of available datasets, and modeling errors.

Keywords: Model updating, nonlinear normal modes, nonlinear system identification, Bayesian inference, modeling errors.

1. Introduction

Finite element (FE) modeling is commonly used for predicting the dynamical response of structural systems to external loading [1]. However, discrepancies always exist between the measured response and those predicted by models, even for the most sophisticated and detailed models. The sources of these discrepancies can be categorized into three groups: (1) modeling errors, e.g., boundary condition or type of nonlinearity; (2) model parameter value errors, e.g., element stiffness or nonlinear coefficient values; and (3) measurement errors, e.g., sensor and cable noise. Model updating is a process to select the optimal values for model parameters to minimize the discrepancies between measurements and model predictions. This process directly addresses the second source of error but can also reduce some of the modeling errors through model class selection.

Model updating: FE model updating methods were initially formulated and used for application to linear elastic structural systems [2, 3] and have been widely used since then (e.g., [4-7]). However, the application of model updating to nonlinear structures is still sparse. Asgarieh et al. [8, 9] applied FE model updating to estimate parameters of material hysteretic models and studied the effects of different data features. Kyprianou et al. [10] employed model updating based on a differential evolution optimization algorithm for tuning the parameters of the Bouc-Wen hysteretic model. Local nonlinearities such as friction, gap or geometrical nonlinearities are other sources of nonlinear behavior in structural systems. The literature includes a few studies on identification of local nonlinearities through model updating. Schmidt [11] proposed an approach for model updating of dynamical systems with local nonlinearities such as Coulomb friction, gaps and local plasticity using time history data utilizing "modal state observers" to determine initial values. In [12, 13], a nonlinear model updating was performed using data from a drop test of a system with nonlinear foam material. The considered data features in these studies included peak acceleration, time of arrival and standard deviation of model error. Hemez and Doebling [14] discussed and compared the performance of modal parameters metric and time domain metric in model updating of several testbeds at Los Alamos National Laboratory. Meyer and Link [15] utilized FE model updating to calibrate the same nonlinear beam as that of this study with a local cubic spring using displacement response and the model was linearized using harmonic balance method. Kerschen and Golinval applied a two-step methodology of nonlinear model updating to a numerical aeroplane-like structure, decoupling the estimation of the linear and nonlinear parameters [16]. Kurt et al. [17, 18] proposed a model updating strategy to update the system parameters of a benchmark system by matching the backbone branches of the frequency-energy plots with the frequency-energy wavelet transforms of experimental time series.

Deterministic vs. Probabilistic: The above reviewed model updating applications were performed in a deterministic sense where an "optimum solution" for updating parameters is obtained. However, the deterministic methods have a few shortcomings that can be addressed in probabilistic approaches. Two of the main shortcomings of deterministic methods are their inability to: (1) solve locally identifiable or unidentifiable inverse problems (i.e., when there is no unique optimum solution), and (2) quantify the uncertainty of updating parameters. Model parameters uncertainties can be caused by the identification or model updating process, measurement noise, and/or the inherent variability of model parameters due to ambient and environmental conditions. Several studies have shown that the in-service environment such as wind speed, rain and temperature could have significant effects on the dynamical properties of structural systems [19, 20]. Therefore, it is preferred to perform model updating in a probabilistic framework such as Bayesian FE model updating. The advantages of Bayesian model updating over deterministic approaches include quantification of uncertainties for updating parameters, propagation of this uncertainty in structural response prediction, and model class selection [21, 22]. Beck et al. [23-25] presented the probability logic and formulation of Bayesian model updating and validation of the proposed framework when applied to numerically simulated data.

Ching and Beck [26] applied Bayesian model updating to the IASC-ASCE benchmark example and treated the mode shapes as extra variables in model updating. Yuen et al. [27] presented Bayesian damage identification of the same IASC-ASCE benchmark under different identifiability conditions: globally identifiable, locally identifiable, and unidentifiable. Muto and Beck [28] employed Bayesian model updating and model class selection for hysteretic structural models. Ntotsios et al. [29] presented Bayesian damage identification of a highway bridge. Behmanesh et al. [30] implemented Bayesian damage identification to the numerical SAC 9-story steel moment frame where they proposed a process to select optimal subset of modes and optimal modal residual weights to mitigate the effects of modeling errors. To account for inherent variability of structural mass and stiffness due to changing in-service conditions, a Hierarchical Bayesian model updating was proposed in [31].

Nonlinear Normal Modes: NNMs are the extension of linear normal modes for nonlinear dynamical systems. NNMs were first defined by Rosenberg as "vibrations in unison" [32, 33]. This definition was later extended to encompass general, non-necessarily synchronous periodic solutions in [34]. NNMs have received attention as they provide a rigorous theoretical framework for interpreting many nonlinear dynamical phenomena [35-39]. NNMs were also shown to predict the behavior of the nonlinear structure at resonance where the risk of failure is the greatest. NNMs may therefore be considered as key nonlinear dynamical features and exploited for nonlinear model updating, as linear normal modes (natural frequencies, mode shapes) have been widely used in linear model updating with great successes [4-7]. Peter et al. [40] pioneered model updating using NNMs in a deterministic approach. It solved a least-squares problem to minimize the difference between measured backbone curves extracted using phase resonance method and their analytical counterparts computed using harmonic balance method, but it could not quantify the model parameters uncertainties which can be overcome by Bayesian approach applied in this study. Hill et al. [41] employed a probabilistic Bayesian identification of the parameters of nonlinear structures based on analytical models to describe the backbone curves. It applied the second-order normal form technique to derive the analytical expressions describing the backbone curves, which was limited to weakly nonlinear systems and introduced additional error into the model of the system since the analytical expressions only provided an approximate solution. These disadvantages do not exist in the proposed study here.

Nonlinear Subspace Identification: Phase resonance method [42-44] is a well-established approach to extract the backbone curves of nonlinear systems using a quadrature criterion between response and excitation. Resonant decay method [42] is a standard phase resonance approach which has the capability of identifying NNMs, one at a time, with high accuracy, but it is time-consuming because of its trial-and-error nature and input frequency tuning process. Recently, new methods have been developed to overcome these issues by using control-based continuation and excitation power quantities in phase resonance testing [43, 44]. The two-step NNM identification method [45], which is applied in this paper, is capable of identifying

multiple NNMs under broadband excitation by combining a frequency-domain nonlinear subspace identification (FNSI) method with numerical continuation approach [46].

This paper presents a FE model updating approach using NNMs residuals. The proposed approach is formulated in both deterministic and Bayesian frameworks and applied to model updating of a cantilever beam model (numerically simulated data) with local nonlinearity. Performance of the method in both formulations is evaluated when the updating results are compared to the nominal values of updating parameters. The broadband excitation input and the corresponding output responses are simulated and polluted with different levels of Gaussian white noise to represent noisy measurements. The FNSI method combined with numerical continuation is employed to identify the first three NNMs of the beam. Shooting method and pseudo-arclength continuation are used to compute NNMs from the FE model. FE model updating is applied to identify the linear parameter (i.e., the Young's modulus E) and nonlinear stiffness parameters of the model in two separate steps. The deterministic model updating approach calibrates the FE model parameters by minimizing an objective function which consists in the difference between model-predicted and identified NNMs from (simulated) data. The Bayesian approach estimated the posterior probability distribution of the updating parameters through Bayesian inference and the principle of maximum entropy [47, 48]. The stochastic simulation method of Markov Chain Monte Carlo is applied to sample the joint posterior probability distribution. The performance of deterministic and probabilistic FE model updating is studied at different levels of measurement noise, number of available datasets, and in the presence of modeling errors.

2. Model updating based on nonlinear normal modes

This paper proposes a model updating strategy to calibrate the nonlinear system model considering the difference between identified NNMs from measured data (simulated in this study) and their counterparts predicted from the numerical model. The procedure of the proposed model updating strategy using NNMs is illustrated in Figure 1 for both deterministic and Bayesian formulations. The first step in the flow chart is the identification of data features (NNMs) from the input-output measurements of the structural system, which is done through the FNSI method and numerical continuation approach. The same data features are also computed using the numerical model through shooting method combined with pseudo-arclength continuation. Note that the proposed model updating method is not limited to the specific NNM identification and computation (from model) methods, other methods like the phase resonance method, harmonic balance method, or other techniques, which are capable of identifying and computing NNMs can also be exploited and incorporated into this model updating framework. The next step is to evaluate the difference between model-predicted and experimentally identified NNMs, and since NNMs are energy dependent, the difference should consider NNMs at different energy levels. Then, two different approaches are formulated to minimize the difference, namely the deterministic approach which involves an iterative optimization technique, and the Bayesian approach which implements a stochastic sampling method. Both

approaches require computation of NNMs for varying values of model parameters to form the residuals/error functions as functions of model parameters.

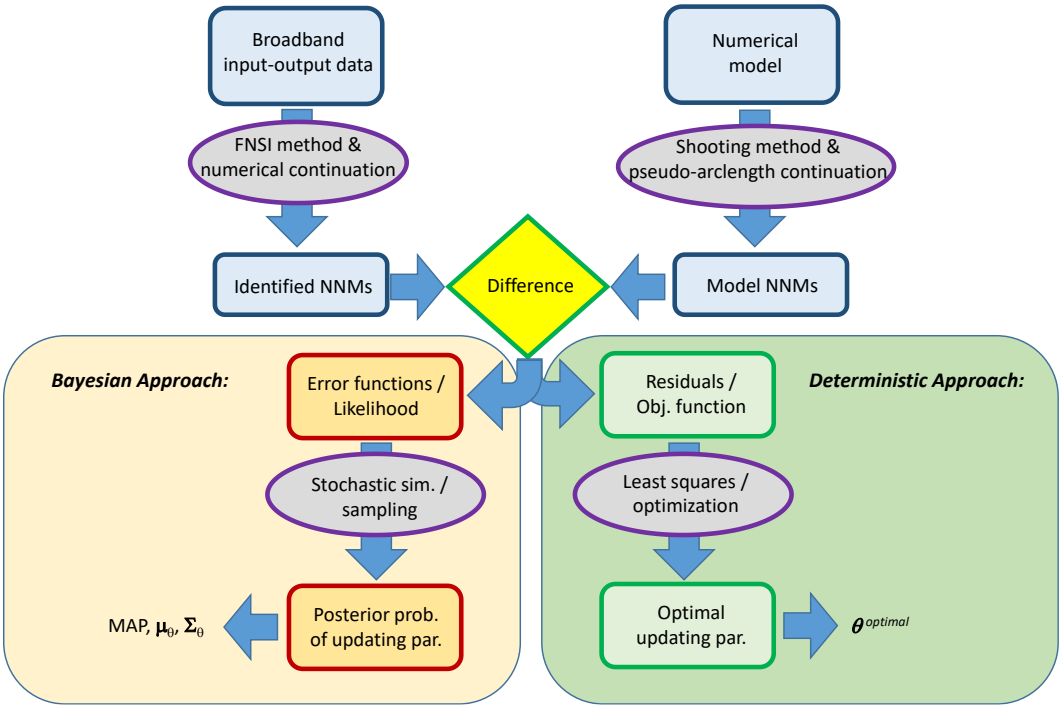

Figure 1. Flowchart of the model updating strategy using NNMs

2.1 Computation of NNMs from numerical model

Defining NNMs as periodic solutions of the conservative equations of motion is appealing as there are numerous methods to compute periodic responses of nonlinear equations [49]. In this study, the shooting method, which is a popular method to solve two-point boundary value problems, is exploited. NNMs form families of periodic solutions that can exhibit bifurcations and internal resonance tongues, which pose challenges to fully track the frequency-amplitude dependence of the NNMs. To address this issue, the shooting method is combined with the pseudo-arclength continuation method, which uses a tangential prediction step and orthogonal correction steps to find and track the evolution of the periodic solutions. The computation of the NNMs is initiated at low energy where NNMs are close to the linear normal modes of the underlying linear system. More details about the method used for the computation of NNMs can be found in [46]. Note also that the proposed model updating method does not rely on the specific use of shooting and pseudo-arclength continuation, and other methods available in the literature could also be used [49].

2.2 Identification of NNMs from experimental data

One of the most popular methods for identification of NNMs is the phase resonance method [42-44]. It has the capability to extract modal parameters from the free-decay response of the

system after turning off the excitation when the system is in resonance at a specified energy level. This method can identify one NNM at a time with high accuracy. This paper applies a different NNM identification approach, i.e., the two-step NNM identification method [45], which is capable of identifying multiple NNMs at a time under broadband excitation by combining a FNSI method with the numerical continuation approach [46].

The first step of the identification approach applies FNSI method to the measured input-output data and derives a state-space model of the system. The input data consists in the broadband excitations in this study and output data could be displacement or acceleration measurements. The FNSI method is a frequency domain method which allows the analyst to focus on specific frequency intervals and discard uninformative data. FNSI can handle multi-input and multi-output systems with high modal density and strong nonlinearities, and does not rely on a preexisting numerical model. Typically, in FNSI, the basis functions used to fit the observed nonlinearities are polynomials or splines, but any linear-in-the-parameter function can be used.

The second step is a numerical continuation approach to compute NNM branches after the state-space model derived from FNSI method is transformed into modal space. This numerical continuation approach uses the same technique of shooting combined with pseudo-arclength continuation, which has been presented in section 2.1. For more details about the two-step NNMs identification method, readers are referred to [45].

2.3 Model updating steps using NNMs

In the model updating process, system parameters such as linear stiffness and nonlinear stiffness parameters are calibrated through an inverse problem to match the model predicted NNMs to the identified ones. For structures with local nonlinearities (as considered in this study), the linear and nonlinear stiffness parameters can be calibrated separately. Indeed, at low energy level, the nonlinear stiffness has very limited influence on the dynamics and the linear stiffness parameters may be updated using the linear normal modes estimated as NNMs at low energy level. After identifying the underlying linear behavior of the system, the nonlinear model parameters can be estimated using NNMs at higher energy levels. This two-step model updating strategy simplifies the inverse problem and mitigates the potential issue of internal resonance and bifurcation of NNMs under different combinations of linear and nonlinear stiffness parameters. The inverse problem can then be solved through a deterministic or a probabilistic/Bayesian formulation.

2.3.1 Deterministic formulation (least-squares)

In the deterministic model updating formulation, a least-squares problem is solved through an iterative optimization algorithm. Model updating is performed by minimizing an objective function which consists of the discrepancies between model-predicted and identified NNMs by adjusting the model parameters. The objective function in this study is defined as

$$f(\boldsymbol{\theta}) = \sum_{m=1}^{N_m} e_\lambda^m(\boldsymbol{\theta}) + \sum_{m=1}^{N_m} e_\phi^m(\boldsymbol{\theta}) \tag{1}$$

in which $\boldsymbol{\theta}$ is the vector of updating parameters, N_m is the total number of modes, $e_\lambda^m(\boldsymbol{\theta})$ and $e_\phi^m(\boldsymbol{\theta})$ are the frequency and mode shape residuals for mode m, respectively.

$$e_\lambda^m(\boldsymbol{\theta}) = \frac{1}{N_p^m} \sum_{i=1}^{N_p^m} \frac{\left(\tilde{\lambda}_{m,i} - \lambda_{m,i}(\boldsymbol{\theta})\right)^2}{\sigma_{\lambda_{m,i}}^2} \tag{2}$$

$$e_\phi^m(\boldsymbol{\theta}) = \frac{1}{N_p^m} \sum_{i=1}^{N_p^m} \frac{1}{\sigma_{\phi_m}^2} \left(\frac{\tilde{\boldsymbol{\Phi}}_{m,i}}{\left\|\tilde{\boldsymbol{\Phi}}_{m,i}\right\|} - a_{m,i} \frac{\Gamma\boldsymbol{\Phi}_{m,i}(\boldsymbol{\theta})}{\left\|\Gamma\boldsymbol{\Phi}_{m,i}(\boldsymbol{\theta})\right\|} \right)^T \left(\frac{\tilde{\boldsymbol{\Phi}}_{m,i}}{\left\|\tilde{\boldsymbol{\Phi}}_{m,i}\right\|} - a_{m,i} \frac{\Gamma\boldsymbol{\Phi}_{m,i}(\boldsymbol{\theta})}{\left\|\Gamma\boldsymbol{\Phi}_{m,i}(\boldsymbol{\theta})\right\|} \right) \tag{3}$$

where $\tilde{\lambda}_{m,i}$ and $\lambda_{m,i}(\boldsymbol{\theta})$ refer to the identified and model predicted eigenfrequency of mode m at energy level i, respectively, with $\tilde{\lambda}_{m,i} = (2\pi \tilde{f}_{m,i})^2$ and $\tilde{f}_{m,i}$ is identified natural frequency of NNMs in Hz. $\tilde{\boldsymbol{\Phi}}_{m,i}$ and $\boldsymbol{\Phi}_{m,i}(\boldsymbol{\theta})$ are the identified and model predicted mode shapes of mode m at energy level i. N_p^m is the total number of energy levels considered at the NNM branch for mode m. $N_p^m = 1$ for estimating linear stiffness parameters since the lowest energy level is considered, and N_p^m = the number of available points on the NNM branches for estimating nonlinear stiffness parameters. $\boldsymbol{\Gamma}$ is the matrix that picks the corresponding components of $\boldsymbol{\Phi}_{m,i}(\boldsymbol{\theta})$ to be compared with the experimentally measured components of $\tilde{\boldsymbol{\Phi}}_{m,i}$. $\sigma_{\lambda_{m,i}}$ and σ_{ϕ_m} are standard deviations of eigenfrequencies and mode shapes which are defined in Eq. (4) and (5). $a_{m,i}$ is scaling factor as defined in Eq. (6).

$$\sigma_{\lambda_m,i} = w_m \mathrm{CoV}_\lambda \tilde{\lambda}_{m,i} \tag{4}$$

$$\sigma_{\phi_m} = \sqrt{N_s}\, w_m \mathrm{CoV}_\lambda \tag{5}$$

$$a_{m,i} = \frac{\tilde{\boldsymbol{\Phi}}_{m,i} \cdot \Gamma\boldsymbol{\Phi}_{m,i}(\boldsymbol{\theta})}{\left\|\tilde{\boldsymbol{\Phi}}_{m,i}\right\| \left\|\Gamma\boldsymbol{\Phi}_{m,i}(\boldsymbol{\theta})\right\|} \tag{6}$$

In Eq. (4) and (5), w_m is the weight assigned for each mode. Weights are usually decided based on the identification uncertainty of each mode, i.e., higher weight is assigned for mode with lower identification uncertainty. In this study, equal weights are assigned for the three NNMs since comparable identification uncertainties are observed. N_s is the number of components in mode shapes which is equal to the number of sensors. CoV_λ is the coefficient-of-variation (ratio of standard deviation to the mean value) of identified eigenfrequencies, averaged over different modes and energy levels.

2.3.2 Probabilistic formulation (Bayesian inference)

This section presents the formulation of probabilistic model updating using Bayesian inference. In this process, the posterior probability distribution of updating parameters is estimated based on the likelihood of parameters given the measured datasets as well as the prior knowledge. This section provides the error functions used in this study and the derivation of the likelihood function. More details about the general formulation of Bayesian model updating can be found in [21-25].

According to Bayes' theorem, the posterior probability distribution of updating parameters given the measured data writes:

$$p(\boldsymbol{\theta} \mid \mathbf{d}, M) = \frac{p(\mathbf{d} \mid \boldsymbol{\theta}, M)\, p(\boldsymbol{\theta} \mid M)}{p(\mathbf{d} \mid M)} \tag{7}$$

In Eq. (7), $p(\boldsymbol{\theta} \mid \mathbf{d}, M)$ is the posterior probability density function (PDF) of updating parameters $\boldsymbol{\theta}$ given measured datasets $\mathbf{d} = [\mathbf{d}_1 \ ... \ \mathbf{d}_N]$, M denotes the considered model class, $p(\mathbf{d} \mid \boldsymbol{\theta}, M)$ is the likelihood function, and $p(\boldsymbol{\theta} \mid M)$ is the prior PDF which reflects the prior knowledge about the updating parameters. In this study, the prior PDFs are assumed to be uninformative, i.e., have uniform distributions. $p(\mathbf{d} \mid M)$ is the evidence which normalizes the posterior PDF. The conditioning on model class M is omitted in the following discussion for brevity.

Based on the principle of maximum entropy [47, 48], Gaussian PDF provides the maximum uncertainty of an unbounded variable with finite mean and variance. Therefore, the prediction error e_i which is the difference between model-predicted and experimentally identified data feature is assumed to follow a zero-mean Gaussian PDF:

$$e_i = \tilde{d}_i - d_i(\boldsymbol{\theta}) \tag{8}$$

$$p(\tilde{d}_i \mid \boldsymbol{\theta}) = p(e_i \mid \boldsymbol{\theta}) = \frac{1}{\sqrt{2\pi}\sigma_i} \exp\left(-\frac{1}{2}\frac{e_i^2}{\sigma_i^2}\right) \tag{9}$$

In this equation, $p(\tilde{d}_i \mid \boldsymbol{\theta})$ is the corresponding likelihood function which has the same distribution as the prediction error (with a moved mean value) for given values of updating parameters $\boldsymbol{\theta}$. $\tilde{d}_i$, $d_i(\boldsymbol{\theta})$ denote the measured and model-predicted data features, i.e., NNMs in this study, and σ_i refers to their corresponding standard deviations evaluated from identified NNMs.

The considered NNM prediction errors in this study include eigenfrequency error and mode shape error, similar to deterministic approach. Assuming that all prediction errors (also referred

to as error functions) are independent, the joint likelihood function given one dataset $\mathbf{d}_n$ can be written as

$$p(\mathbf{d}_n \mid \boldsymbol{\theta}) = \prod_{i=1}^{n_i} p(\tilde{d}_i \mid \boldsymbol{\theta}) = \prod_{i=1}^{n_i} \frac{1}{\sqrt{2\pi}\sigma_{d_i}} \exp(-\frac{1}{2}\frac{e_{d_i}^2}{\sigma_{d_i}^2}) \propto \exp\left(-\frac{1}{2} J(\boldsymbol{\theta}, \mathbf{d}_n)\right) \tag{10}$$

$$\text{with } J(\boldsymbol{\theta}, \mathbf{d}_n) = \sum_{m=1}^{N_m} e_{\lambda}^m(\boldsymbol{\theta}) + \sum_{m=1}^{N_m} e_{\phi}^m(\boldsymbol{\theta}) \tag{11}$$

In the case of having multiple independent datasets of system identification results, the likelihood function can be expressed as:

$$p(\mathbf{d}_1 : \mathbf{d}_N \mid \boldsymbol{\theta}) \propto \prod_{n=1}^{N} \exp\left(-\frac{1}{2} J(\boldsymbol{\theta}, \mathbf{d}_n)\right) = \exp\left(\sum_{n=1}^{N} -\frac{1}{2} J(\boldsymbol{\theta}, \mathbf{d}_n)\right) \tag{12}$$

The posterior PDF is then formulated as Eq. (13) when the prior distributions are assumed to be uniform.

$$p(\boldsymbol{\theta} \mid \mathbf{d}) = \hat{c} \exp\left(\sum_{n=1}^{N} -\frac{1}{2} J(\boldsymbol{\theta}, \mathbf{d}_n)\right) \tag{13}$$

where $\hat{c}$ is a constant. Evaluating the posterior PDF in Eq. (13) analytically is a challenging task because computing the unknown constant $\hat{c}$ requires solving high dimensional integrals. Markov Chain Monte Carlo (MCMC) methods can evaluate Eq. (13) numerically without needing to compute the constant.

By comparing the deterministic objective function in Eq. (1) and Eq. (11) in the Bayesian approach, it can be seen that they have the same formulation of residuals/error functions. Therefore, the optimal values of updating parameters from deterministic approach would coincide with the maximum a-posterior (MAP) values of the Bayesian approach if the same datasets are used in both approaches, i.e., the optimal values which minimize Eq. (1) will maximize the posterior probability function of Eq. (13). Note that no regularization term is considered in Eq. (1) which corresponds to consideration of uniform (uninformative) prior distribution in Eq. (13). In case of having an informative prior in the Bayesian approach, a regularization term should be added in the corresponding deterministic objective function so the optimal deterministic and MAP values coincide as it is shown in [50].

3. Numerical evaluation of the proposed framework

3.1 Description of the considered structure

To verify and evaluate the performance of the proposed model updating strategy, an application to numerically simulated data of a nonlinear beam is considered. The nonlinear beam

is a numerical model of the COST Action F3 benchmark shown in Figure 2(a) [51, 52]. The benchmark consists of a main beam with one end clamped to the base, the other end connected to a thin beam using a bolt. For the purpose of simulating measured data, force sensor and accelerometers are considered on the beam as they were used in an actual test to measure the input excitation force and acceleration response of the beam. In Figure 2(a), A_1~A_7 refer to seven accelerometers and F_1 refer to input force sensor. In this study, a representative FE model of the beam (shown in Figure 2(b)) is used to simulate its nonlinear response to periodic broadband excitations. The numerically simulated data of the beam are used for evaluation of the proposed model updating approach since it allows studying the effect of controlled levels of modeling error and measurement noise on the updating results. Based on the experimental study and physical examination of the beam, the following modeling and discretization strategy is employed: the left end of the main beam is modeled as a pin support with a rotational spring of stiffness k_1; the connection of two beams is modeled with a lumped mass of 11.15 g (the mass of the bolt connection) and a rotational spring of stiffness k_2; the right end of the thin beam is considered as a pin support with a soft rotational spring of stiffness k_3; the main and thin beams are discretized into 14 and 3 two-dimensional Euler-Bernoulli beam elements, respectively. Seven accelerometers are modeled as lumped masses with 2.1 g each. According to the dynamical test of the beam, a local nonlinearity at the connection of the two beams is introduced by the large displacement of the thin beam, leading to a nonlinear geometrical effect, and a small asymmetry in the thin beam requires the introduction of a quadratic term in addition to the cubic term, in order to capture the softening-hardening behavior observed experimentally [52]. The nonlinear coefficients c_1 and c_2 are assigned for the cubic and quadratic terms, respectively. The geometrical and mechanical properties of the FE model are summarized in Table 1 and Table 2, respectively.

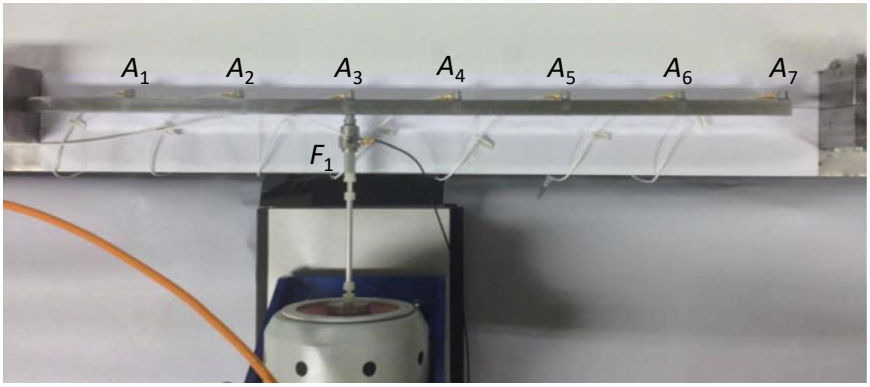

(a)

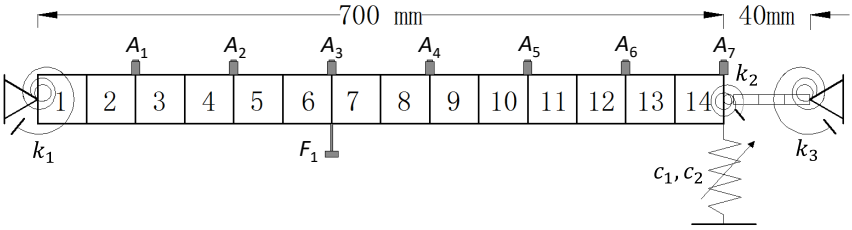

(b)

Figure 2. (a) Test setup of the benchmark beam at University of Liege (taken from [52]); (b) FE model of the nonlinear beam used for numerical simulation of data

For the studied nonlinear beam, three updating parameters are considered to represent the linear and nonlinear stiffness parameters: the Young's modulus E, and the nonlinear coefficients c_1 and c_2. Note that the stiffness k_1, k_2, k_3 of the rotational springs are not updated together with E since they would make the inverse problem ill-conditioned. However, to study the effect of modeling errors, a case where the values of k_1, k_2, k_3 are assumed as infinity (i.e., perfectly rigid connections) will be considered. The nominal values of the three updating parameters are shown in Table 2. In the first step of the proposed two-step modeling updating strategy, the Young's modulus is estimated using NNMs at the lowest energy level, while the whole NNM branches are used to estimate the nonlinear coefficients c_1 and c_2 in the second step.

Table 1. Geometrical properties of the FE model

	Length (mm)	Thickness (mm)	Width (mm)
Main beam	700	14	14
Thin beam	40	0.5	14

Table 2. Mechanical properties of the FE model

Young's modulus E (Pa)	Density (kg/m^3)	k_1 (N/rad)	k_2 (N/rad)	k_3 (N/rad)	c_1 (N/m^3)	c_2 (N/m^2)
2.05×10^{11}	7800	114700	42.2	40	8×10^{9}	-1.05×10^{7}

The two-step identification process is applied to the simulated measurements to identify the first three NNMs. To study the effect of noise on identified NNMs, the simulated sensor responses are polluted with three different noise levels, namely 1%, 2% and 5%. The added noise is Gaussian white noise with standard deviation equal to the noise level (e.g., 1%) multiplied by the root-mean-square (RMS) of acceleration response at the tip of the main beam. Independent Gaussian white noise vectors are added to the simulated time histories at the location of the seven accelerometers. For each noise level, 20 sets of NNMs are identified with independent realizations of added noise. Figure 3 shows the frequency-energy plots of the identified NNMs under different noise levels and mode shapes at energy levels corresponding to tip displacements of 0.01 mm, 0.5 mm and 0.95 mm. The mode shapes are normalized to make the tip displacements equal to unity. It can be observed that the identified NNM branches exhibit softening-hardening behavior with larger frequency discrepancies for the higher noise levels; mode shapes of NNM 2 and 3 evolve significantly with energy level, but no evident change can be seen for NNM 1.

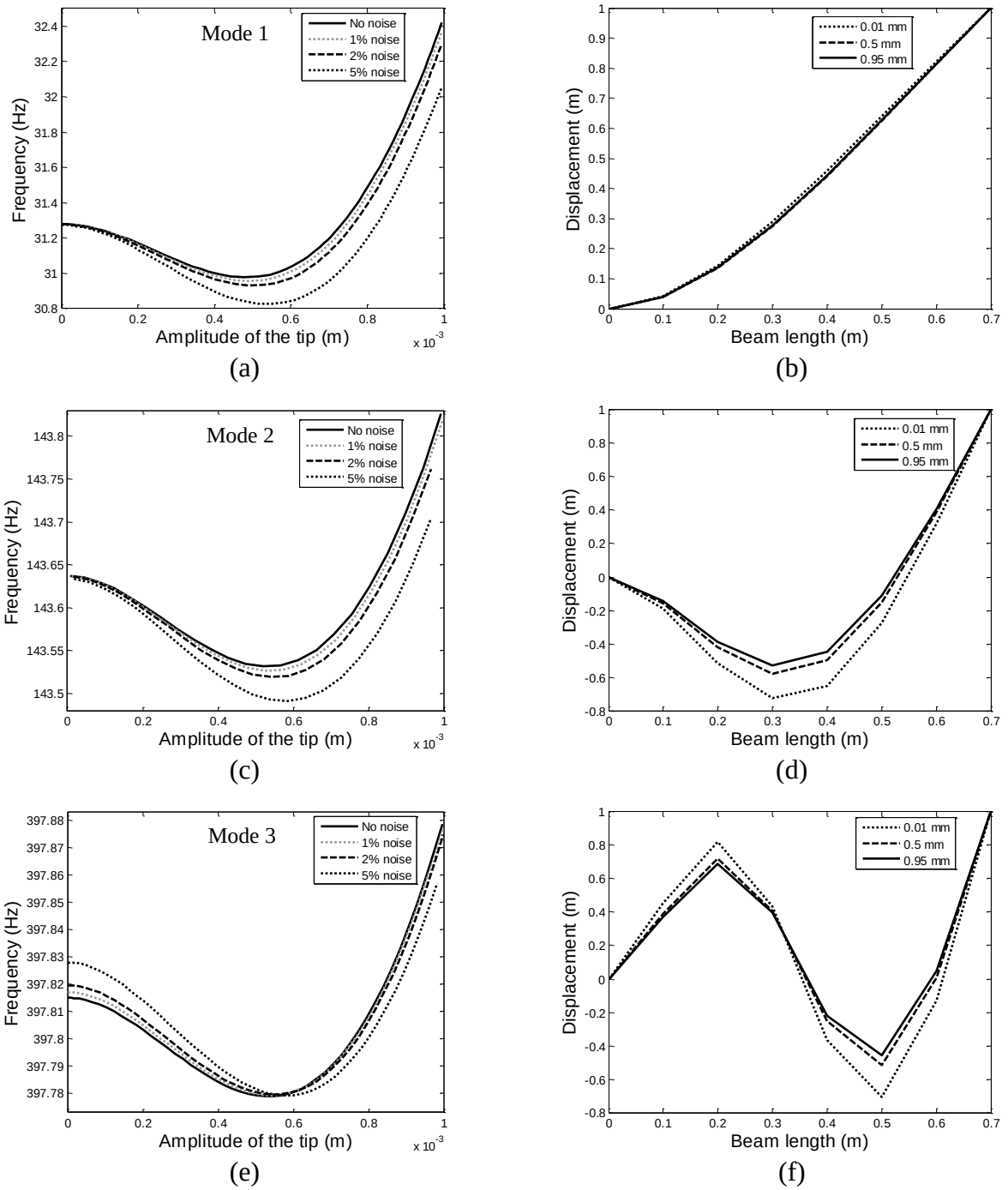

Figure 3. (a, c, e): Frequency-energy plots of identified NNM 1, 2 and 3 with different noise levels (only one dataset is shown for each noise level); (b, d, f): identified mode shapes (1% noise) at energy levels corresponding to tip displacements of 0.01 mm, 0.5 mm and 0.95 mm (mode shapes are normalized to make the tip displacement equal to one)

3.2 Deterministic model updating results

This section presents the model updating results when using the deterministic formulation for the three considered noise levels and 20 independent noise vector realizations at each level. The optimization is performed in MATLAB [53] using the built-in interior point optimization algorithm [54], which does not require the gradients of the objective function with respect to the updating parameters. In solving the least-squares problem, the updating parameters are constrained to avoid instability in the inverse problem. Table 3 summarizes the initial values of the updating parameters and their considered bounds in the optimization process. Note that the reported values are normalized to their nominal (exact) counterparts. The initial values are intentionally selected to be far from the exact values. These far-off initial guesses make sure good estimates of the updating parameters can be achieved even if the initial guess is not close to the true values. For simple systems, better initial guesses can be obtained using simple identification techniques, or curve fitting the NNMs [41, 43]. Large bounds account for big prior uncertainties of the updating parameters (smaller bounds would facilitate optimization process if prior knowledge is available).

Table 3. Initial guesses and bounds of updating parameters

	E/E^{exact}	c_1/c_1^{exact}	c_2/c_2^{exact}
Initial guess	0.2	1.8	0.2
Lower bound	0.1	0.1	0.1
Upper bound	3	2	2

For each noise level, deterministic model updating is performed to adjust the initial FE model parameters to match each of 20 datasets of identified NNMs, resulting in 20 sets of updating parameters. The results are shown as boxplots in Figure 4, where the bottom and top of the boxes denote the first and third quartiles, the lower and the upper end of the whisker denote the lowest and highest values within 1.5 interquartile range of the lower and upper quartile, respectively, the line in the middle of the box denotes median, and the black circle indicates the mean value. The statistics of deterministic model updating results are summarized in

Table 4. It can be observed that: (1) the Young's modulus E is estimated very accurately with very small variability, which is due to the small uncertainty in the identified linear normal modes (estimated as NNMs at the lowest energy level), as shown in Figure 3; (2) c_1 and c_2 are estimated closely to their true values but with larger variability than E, and the largest variability is observed for the coefficient of the quadratic term, c_2, which is due to the large identification uncertainty in the NNMs at higher energy levels; (3) small bias is observed for both c_1 and c_2 which comes from the error in the two-step NNM identification process; and (4) in general, larger variability is observed for higher noise levels.

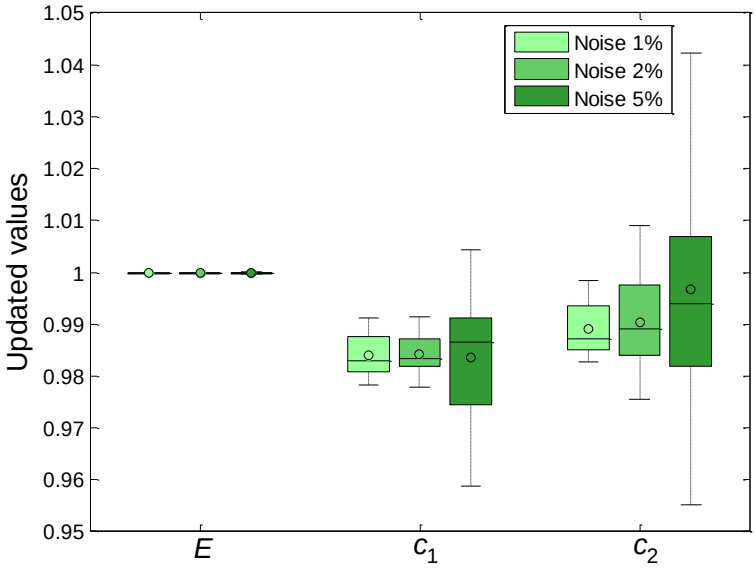

Figure 4. Boxplot of deterministic model updating results

Table 4. Statistics of deterministic model updating results

Noise level		E/E^{exact}	c_1/c_1^{exact}	c_2/c_2^{exact}
1%	Mean	0.9999	0.9839	0.9891
	Std	2.39×10^{-5}	0.0039	0.0054
2%	Mean	0.9999	0.9841	0.9903
	Std	4.87×10^{-5}	0.0037	0.0083
5%	Mean	0.9999	0.9837	0.9967
	Std	1.13×10^{-4}	0.0117	0.0223

Note: Std means standard deviation.

3.3 Bayesian model updating results

The Bayesian model updating approach is implemented for estimation of the three considered model parameters for three noise levels and four different dataset numbers (N_d = 1, 5, 10, or 20), resulting in $3\times4=12$ cases of Bayesian model updating. For the case of a single dataset (N_d = 1), the average NNMs over the total 20 datasets are used. For 5, 10 and 20 datasets cases (N_d = 5, 10, 20), the first 5, 10 and all 20 datasets of identified NNMs are considered.

The first step of Bayesian model updating is to estimate the Young's modulus E using NNMs at the lowest energy level. A Markov Chain Monte Carlo (MCMC) approach is implemented to sample the posterior probability distribution formulated in section 2.3.2. Unlike Monte Carlo method which estimates the probability distribution by drawing independent samples, the MCMC method builds a Markov Chain which eventually converges to the static distribution (posterior PDF). The Markov Chain starts with an initial guess which is not necessarily in the high probability region of the static distribution but after the initial transition steps the chain will

converge to the static distribution given that enough samples are generated. The Metropolis-Hastings (MH) algorithm [55, 56] is chosen for the MCMC sampling of the Young's modulus E. A Gaussian distribution is used as the proposal distribution in the MH algorithm and its standard deviation is selected such that acceptance ratio of samples in the algorithm becomes close to 40%, as suggested by [57] to provide the optimal sample estimations. A burn-in strategy is utilized to remove the initial transitional samples to give a better estimate of parameter distribution. The generated sample statistics after the burn-in period are reported in Table 5 for different noise levels and dataset numbers. It can be observed that the sample means are very close to the exact values of E and the sample standard deviations are very small in all cases indicating very low estimation uncertainty. It can also be seen that the standard deviation increases for higher noise levels, while it is reduced as more datasets are used in the updating process. This can also be seen in Figure 5 that shows the standard deviation of posterior PDF of E as a function of dataset numbers and different noise levels. Figure 6 plots histogram of the samples of E and evolution of sample statistics for 2% noise level and $N_d = 1$ after burn-in. It can be seen that the Markov Chain converges to the high probability region after the first few thousand samples and the sample mean and standard deviation tend to stay constant as more samples are generated. This confirms that the number of samples used in this study is sufficient to give accurate estimation for the posterior PDF of E.

Table 5. Sample information and statistics of Bayesian model updating of E

Noise level \ N_d		1	5	10	20
1%	Num. of samples	100,000	200,000	200,000	200,000
	Burn-in	10,000	20,000	30,000	30,000
	Sample mean	0.9999	0.9999	0.9999	0.9999
	Sample std	2.36×10^{-4}	1.05×10^{-4}	7.43×10^{-5}	5.25×10^{-5}
2%	Num. of samples	100,000	200,000	200,000	200,000
	Burn-in	10,000	20,000	30,000	30,000
	Sample mean	0.9999	0.9999	0.9999	0.9999
	Sample std	4.61×10^{-4}	2.06×10^{-4}	1.46×10^{-4}	1.03×10^{-4}
5%	Num. of samples	100,000	200,000	200,000	200,000
	Burn-in	10,000	20,000	30,000	30,000
	Sample mean	0.9999	0.9999	0.9999	0.9999
	Sample std	1.16×10^{-3}	5.23×10^{-4}	3.68×10^{-4}	2.60×10^{-4}

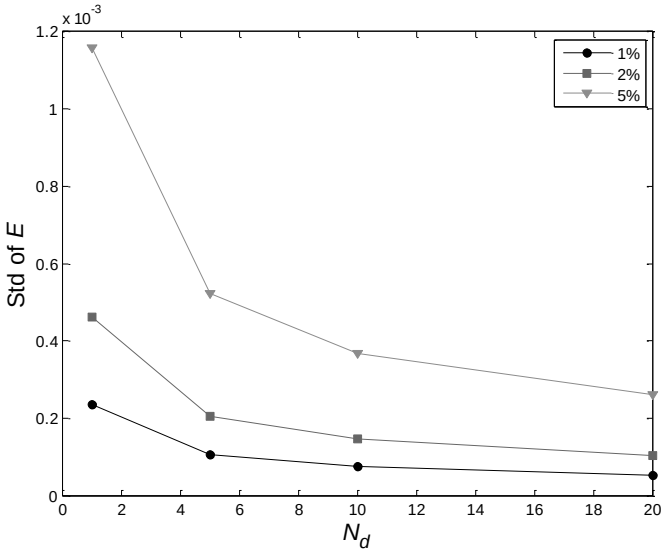

Figure 5. Posterior standard deviation of E for different noise levels and dataset numbers

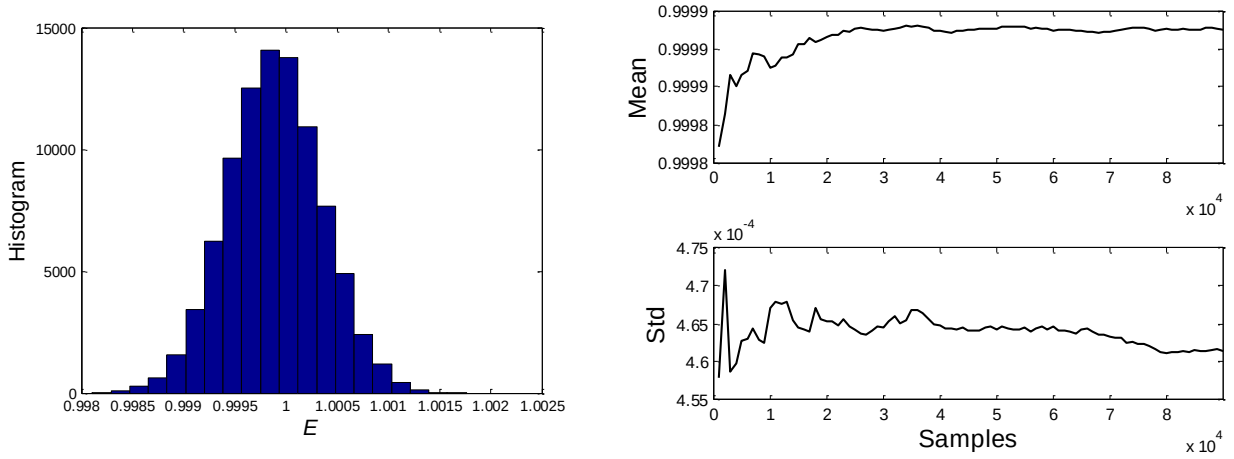

(a) (b)

Figure 6. (a): Histogram of samples of E; (b): mean and standard deviation excluding burn-in samples

After the Young's modulus E is estimated in the first step, the nonlinear coefficients c_1 and c_2 are estimated in the second step using the complete NNM branches. Since the estimated uncertainty of E is very small, the value of Young's modulus is fixed at the most probable value (the same value as MAP) in the second step. The Transitional Markov Chain Monte Carlo (TMCMC) [58] method is used to sample the joint posterior probability distribution of c_1 and c_2. It is worth noting that the MH algorithm was not effective for sampling the joint posterior PDF of c_1 and c_2 which has a more complex form and is more challenging to sample. The MH algorithm was initially implemented but could not generate enough samples at the high probability regions of the posterior PDF. TMCMC is a powerful tool to sample complex functions such as multimodal functions and those with highly localized peaks (as in this study). The key idea of TMCMC is that it creates a series of intermediate posterior PDFs and utilizes sampling and resampling strategies to make samples move step by step to high probability

regions, avoiding directly sampling the final posterior PDF, which may be numerically challenging to do in a single step. Another advantage of TMCMC is that it is capable of estimating the evidence function $p(\mathbf{d}\,|\,M)$ which can be used for model class selection and hyper robust response prediction through model class averaging [58].

In the application of TMCMC method, through a trial and error process, and to create a smooth transition between intermediate PDFs and reduce computation effort, seven intermediate PDFs $p_j(\boldsymbol{\theta}\,|\,\mathbf{d})$ are considered as shown in Eq. (14):

$$p_j(\boldsymbol{\theta}\,|\,\mathbf{d}) \propto p(\boldsymbol{\theta}) \cdot p(\mathbf{d}\,|\,\boldsymbol{\theta})^{s_j} \qquad j=1,...,7 \tag{14}$$

The power s_j of different stages are selected as 0, 1e-5, 1e-3, 0.1, 0.2, 0.5 and 1, with the last stage $p_7(\boldsymbol{\theta}\,|\,\mathbf{d}) = p(\boldsymbol{\theta}\,|\,\mathbf{d})$. The prior PDF $p(\boldsymbol{\theta})$ is assumed to be a joint uniform distribution over the area of $0.1 \le c_1, c_2 \le 2$. One thousand samples are generated in each stage of TMCMC. Figure 7 plots the samples at stages 1 to 7 for the case of 2% noise level and N_d = 1. The zoom-in plot of the final stage shows the superposition of 1%, 2% and 5% noise level results. It can be seen that: (1) at stage 1, the samples are uniformly distributed in the space as the prior PDF is assumed to be uniform; (2) samples quickly converge to the high probability area as the stage power s_j increases; (3) at the final stage, all the samples are concentrated in a very small area close to the exact values, which means the nonlinear coefficients c_1 and c_2 are estimated accurately with small uncertainty; and (4) a strong correlation, indicated by the angle of the point cloud, is observed between c_1 and c_2 as shown in the zoom-in plot of the final stage. The correlation is positive because an overestimation of one nonlinear coefficient leads to an increase in the other coefficient to compensate. Note that the nonlinear coefficients are normalized by their nominal values and therefore, an increase in c_2 would mean a decrease in its real value since its nominal value is negative. The histogram and kernel marginal PDFs of c_1 and c_2 are shown in Figure 8. It can be seen that the marginal PDFs of c_1 and c_2 are close to Gaussian distributions. The sample statistics and correlation coefficient between c_1 and c_2 in all cases are reported in Table 6. It is observed that: (1) means of c_1 and c_2 in all cases are very close to the exact values with slight bias observed due to the identification errors of NNMs, as observed in the deterministic case. (2) Noise level and dataset amount N_d do not have a significant influence on the estimation bias. (3) Standard deviations of c_1 and c_2 increases with higher noise level. However, the standard deviations are generally reduced with more datasets used as shown in Figure 9. (4) The correlation coefficients between c_1 and c_2 are close to 1, indicating very strong correlation between these two modeling parameters, as explained above.

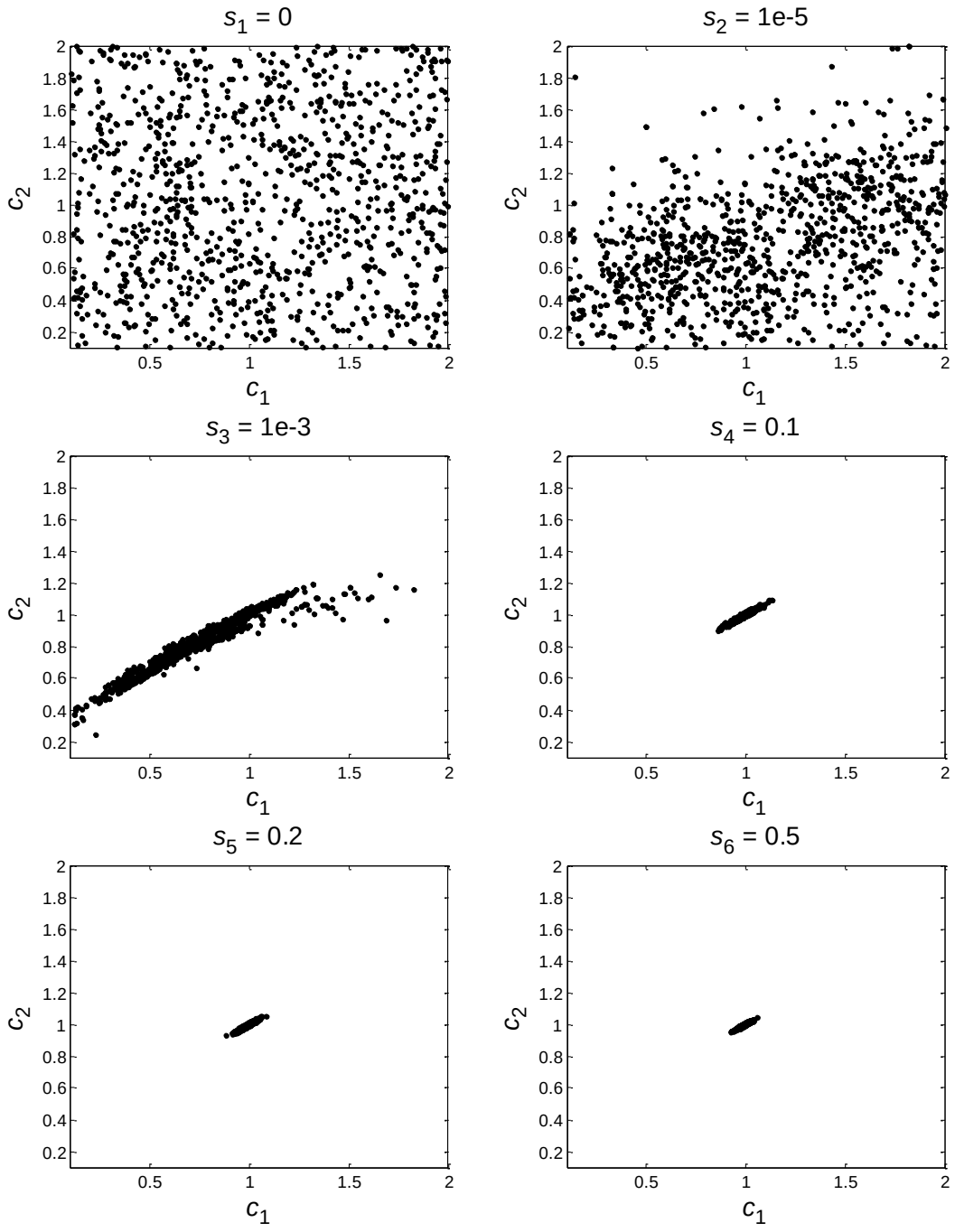
s_1 = 0
s_2 = 1e-5
s_3 = 1e-3
s_4 = 0.1
s_5 = 0.2
s_6 = 0.5
c_1
c_2

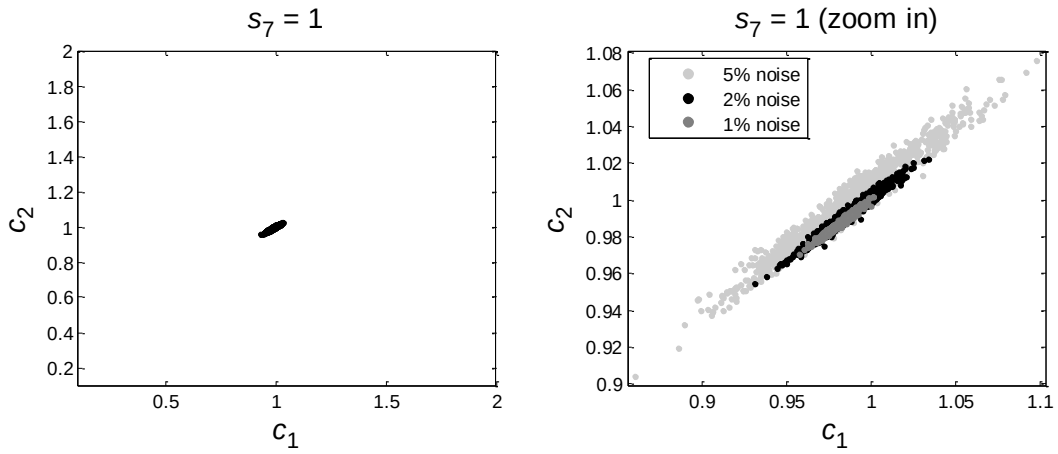

Figure 7. Transitional samples at each stage with 2% noise level and N_d = 1 (with results from 1% and 5% noise levels superimposed in the zoom-in plot of final stage)

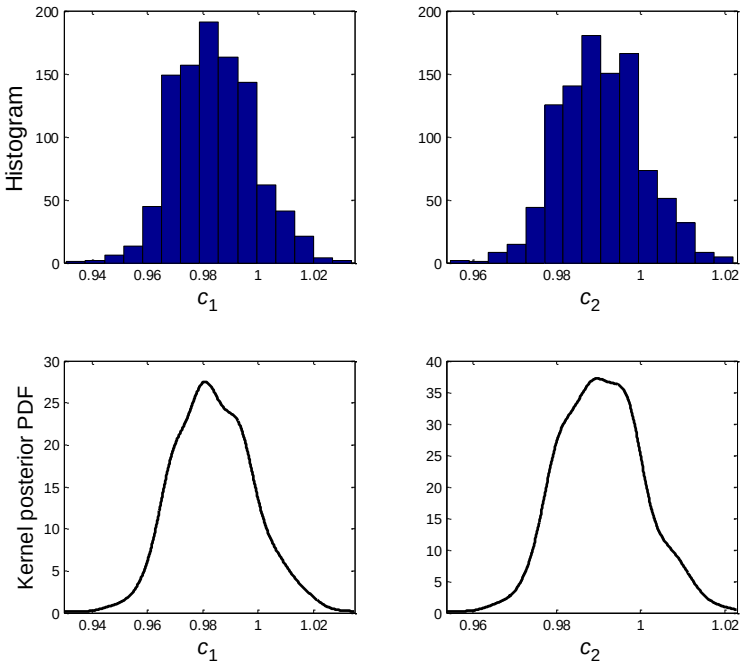

Figure 8. Histogram and kernel posterior marginal PDFs of c_1 and c_2 with 2% noise level and N_d = 1

Table 6. Sample statistics of Bayesian model updating results of all cases

Noise level	N_d	1	5	10	20
1%	c_1 mean / std (%)	0.981 / 0.65	0.982 / 0.18	0.981 / 0.18	0.983/ 0.18
	c_2 mean / std (%)	0.987 / 0.46	0.990 / 0.11	0.988 / 0.12	0.988 / 0.13
	ρ	0.98	0.94	0.97	0.97
2%	c_1 mean / std (%)	0.984 / 1.41	0.986 / 0.79	0.981 / 0.39	0.979 / 0.33
	c_2 mean / std (%)	0.991 / 0.99	0.995 / 0.54	0.989 / 0.25	0.986 / 0.24
	ρ	0.98	0.99	0.97	0.98
5%	c_1 mean / std (%)	0.985 / 3.46	0.976 / 1.17	0.985 / 0.91	0.985 / 0.74
	c_2 mean / std (%)	0.998 / 2.47	0.998 / 0.79	1.000 / 0.61	0.997 / 0.51
	ρ	0.98	0.97	0.97	0.97

Note: ρ indicates the correlation coefficient between c_1 and c_2.

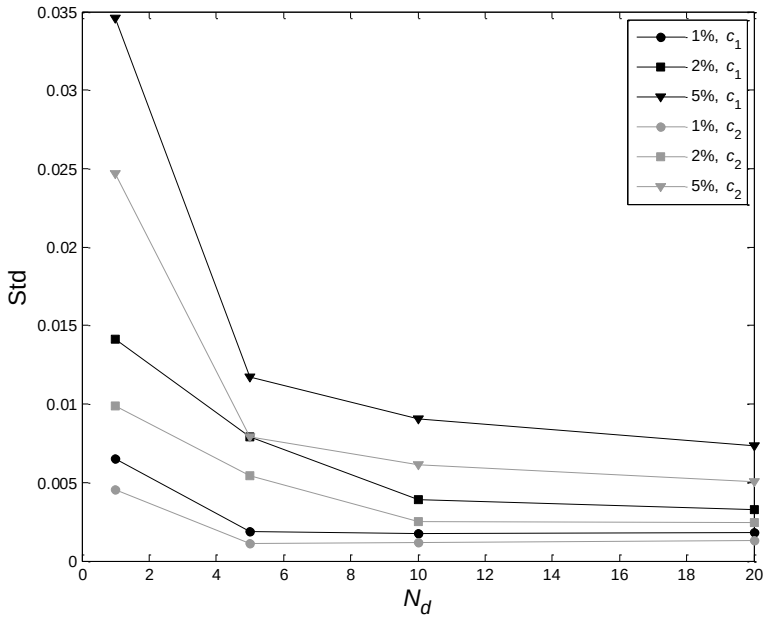

Figure 9. Comparison of standard deviations of different cases

As stated before, the objective function used in the deterministic approach has the same formulation as Eq. (11) used in Bayesian formulation. Therefore, the optimal values of updating parameters from deterministic approach coincide with the MAP value of the Bayesian approach when the same datasets are used. However, the optimal values obtained in section 3.2 are not exactly the same as the results of Bayesian approach with N_d = 1 in section 3.3, because the latter approach uses the average values of 20 datasets of NNMs while the deterministic approach uses one of the 20 datasets each at a time. Note that the obtained standard deviations from the two approaches are not comparable because they represent different uncertainties. The standard deviation of the deterministic approach reflects the variability of system identification results across different datasets and would converge to a non-zero value with increasing datasets. However, the estimated standard deviation in the Bayesian approach represents the estimation

uncertainty of optimal values in the view of measured data and would consistently be reduced as more data are used in the algorithm. In terms of the computational cost, the optimization process in deterministic approach requires approximately 150 iterations to converge resulting in a total of $150 \times 20 = 3000$ for the 20 datasets. In application of the TMCMC algorithm, 1000 samples are generated at each stage requiring a total of 6000 samples, making the Bayesian approach computationally more expensive. However, it should be noted that the implemented optimization approach in the deterministic case is a local method and is not capable of finding the global optimal solution in the case of non-convex and multi-modal objective function while the TMCMC is robust for finding the global optima in a non-convex and multi-modal objective function.

3.4 Bayesian model updating with modeling error

Modeling errors are inevitable in structural dynamics due to simplification, idealization and discretization assumptions used in the modeling process. Such errors pose a significant challenge in response prediction of complex dynamical systems. In the Bayesian model updating framework, statistics (mean and variance) of the error functions provide a measure of modeling error that can be used in model predictions. In this study, two cases of modeling errors are considered. In the first case, the boundary conditions of the beam are considered to be rigid at the left and right end (k_1, $k_3 = \infty$), and the connection of the main and thin beams is assumed to be perfect ($k_2 = \infty$). This model represents the case with wrong assumptions regarding the underlying linear model but correct form of nonlinearity. The second case of modeling error assumes the correct underlying linear model but neglects the quadratic term in the local nonlinearity, i.e., a cubic spring with coefficient c models the original combination of cubic and quadratic terms. The same two-step Bayesian model updating process is employed to identify the linear stiffness parameter Young's modulus E and the nonlinear coefficients c_1 and c_2 for the first case and c for the second case. The effects of modeling errors are studied for the case of 2% noise level and 1 dataset.

3.4.1 Modeling error in boundary conditions ($k_1 = k_2 = k_3 = \infty$)

For modeling error case 1, the stiffness of rotational springs, k_1, k_2 and k_3 are assumed to be infinity. Similar to the case of no modeling error, in the first step of Bayesian model updating, the MH algorithm is used to sample the posterior PDF of the Young's modulus E. A total of 2×10^5 samples are generated and their statistics are shown in Figure 10. The sample mean and standard deviation are reported in Table 7. It can be seen that the Young's modulus is underestimated to compensate for the stiffer boundary conditions. In the second step, the Young's modulus is fixed at its MAP value, and nonlinear parameters c_1 and c_2 are estimated using total NNM branches. The TMCMC method is applied again to sample the joint posterior PDF of c_1 and c_2 with the same 7 intermediate stages considered in section 3.3. The samples at the final stage are shown in Figure 11, with samples from previous no modeling error case superimposed. It can be observed that there is an evident estimation bias for c_1 and c_2 due to

modeling error in the underlying linear model. Strong correlation can still be observed for these two parameters similar to previous case.

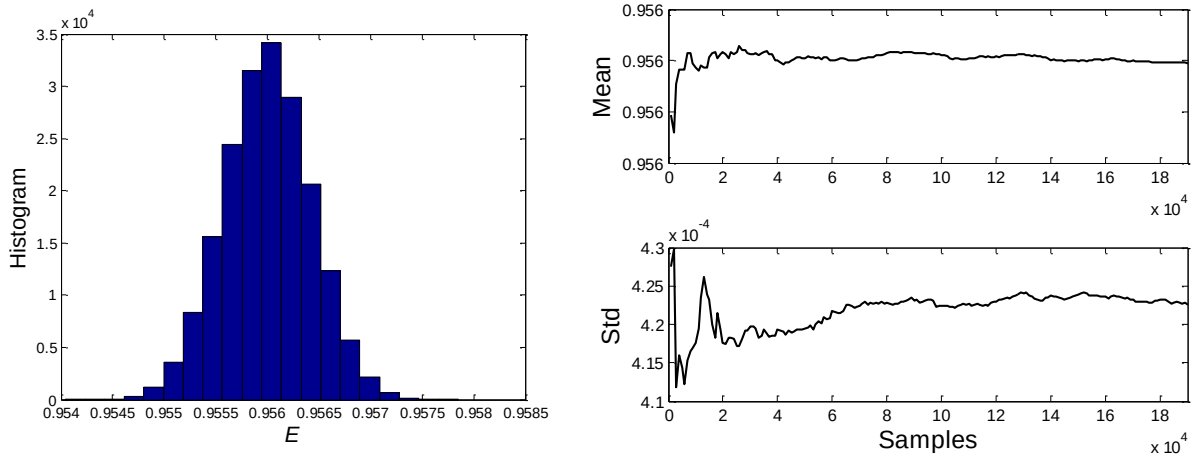

(a) (b)

Figure 10. (a): Histogram of samples of E; (b): sample mean and standard deviation after burn-in

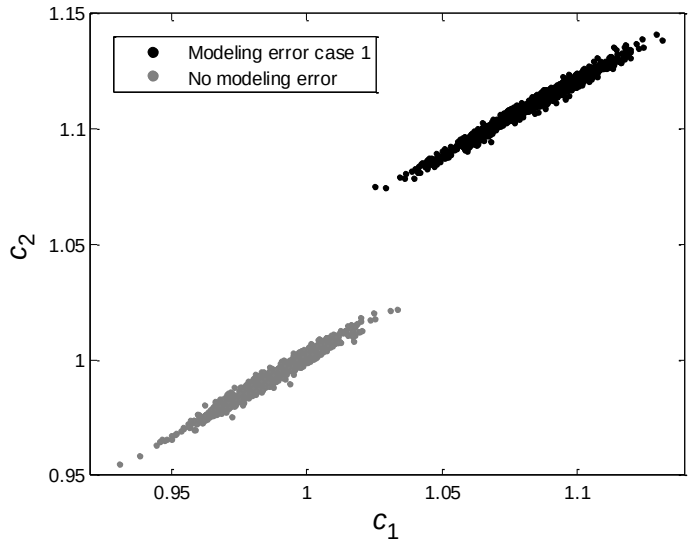

Figure 11. Samples for modeling error case 1 at the final stage with 2% noise level and $N_d = 1$ (samples from previous no modeling error case are superimposed)

Table 7. Sample statistics of E, c_1 and c_2 (modeling error case 1)

	E/E^{exact}	c_1/c_1^{exact}	c_2/c_2^{exact}
Sample mean	0.9560	1.085	1.111
Sample std (%)	4.23×10^{-2}	1.81	1.19

Note: For E, mean and std are calculated after burning in the first 10,000 samples.

3.4.2 Modeling error in local nonlinearity

For the second case of modeling error, the underlying linear model is exact and therefore, the first step of updating of Young's modulus E will provide the same result as in section 3.3. For the second step of estimating the nonlinear coefficient c (which is normalized to the nominal value of c_1 in Table 2), through similar trial and error process and to reduce computation time, seven intermediate PDFs with the power s_j of each stage equal to 0, 1e-3, 0.02, 0.1, 0.2, 0.5 and 1 are considered in TMCMC algorithm. A total of 1000 samples are generated at each stage. The histograms of transitional samples at stages 1-4 and 7 are shown in Figure 12. It can be observed that the samples converge to high probability area very quickly and the variability of samples at the final stage is small. The sample mean and standard deviation at the final stage is equal to 0.07 and 0.0031. The mean value is significantly different from the exact value of c_1 which is expected since the nonlinearity is modeled differently and a cubic spring alone cannot possibly reproduce the softening-hardening behavior caused by quadratic and cubic terms combined.

The estimated evidence $p(\mathbf{d} \mid M_j)$ of the calibrated models for both cases of modeling errors and the case without modeling error are computed and reported in Table 8. Larger evidence indicates the corresponding model is more probable in the view of measured data. It can be seen that the evidence of the two calibrated models with modeling errors are considerably smaller compared to the model without modeling error. Also, among the two cases of modeling errors, the model with error in boundary conditions is more probable than the model with missing nonlinear quadratic term. Note that computation of evidence is usually a challenging task; however, the implemented TMCMC algorithm is capable of providing model evidence as a by-product with no additional computation cost. Recently studies in [59, 60] show that the TMCMC method provides slightly biased estimates for the evidence. However, the biased estimates will not affect the qualitative results presented in this paper since the evidence estimates for each model class are far apart, as denoted in Table 8.

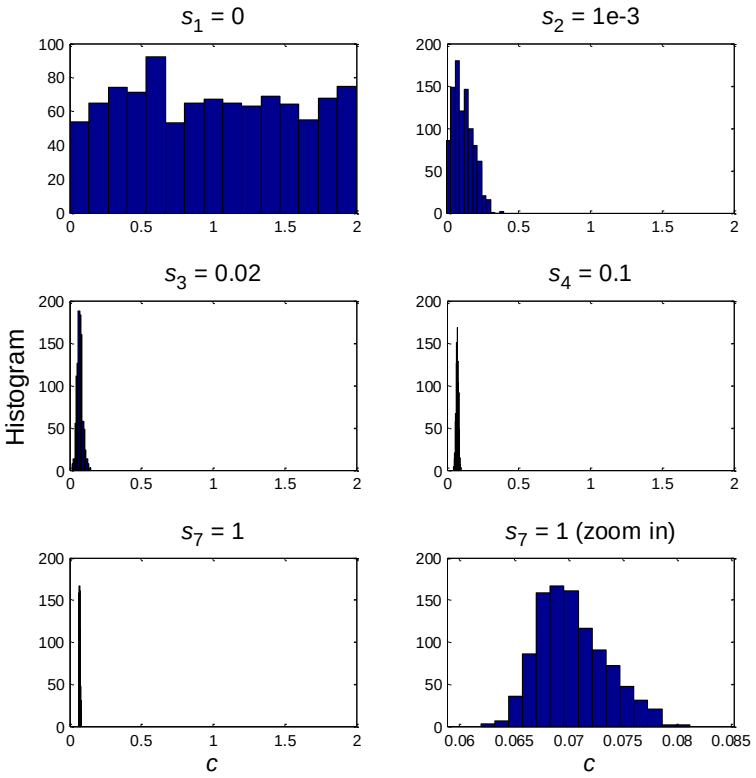

Figure 12. Histogram of transitional samples of nonlinear coefficient c for modeling error case 2 at stages 1-4 and 7

Table 8. Estimated evidence of different model classes

Model class	Evidence $\log(p(\mathbf{d}\mid M))$
Correct model	32.3
Modeling error case 1 (wrong underlying linear model)	-205.5
Modeling error case 2 (wrong nonlinearity)	-2292.9

4. Conclusions

A model updating strategy using NNMs is proposed and evaluated when applied to a numerical nonlinear beam model. The FNSI method combined with a numerical continuation approach is employed for identification of NNMs from simulated data while shooting method combined with pseudo-arclength continuation approach is used to compute NNMs from the model. A two-step model updating strategy is proposed to identify the linear stiffness parameter in the first step and the nonlinear stiffness parameters in the second step to simplify the inverse problem. Two model updating approaches are formulated and implemented in the paper, namely a deterministic approach and a Bayesian approach. In the Bayesian approach, stochastic simulation methods are used to sample the posterior probability distribution of updating parameters: MH algorithm is used for estimating Young's modulus E and TMCMC algorithm is used for estimating c_1 and c_2. The numerical application to the nonlinear beam shows that both deterministic and Bayesian approaches are capable of estimating the updating parameters accurately in the case of no

modeling errors, and the estimation uncertainties increase for higher noise level. However, using more datasets will reduce the estimation uncertainty for the Bayesian formulation while it is not the case for the deterministic approach. In both formulations, small estimation bias is observed due to the NNMs identification error. It is important to note that the model updating results are very sensitive to the estimation error (bias) of NNMs, however, the implemented NNM identification method can handle measurement noise in the form of zero-mean Gaussian white noise relatively well. In a case where noise is caused by unmeasured input disturbances, the NNMs are expected to be identified with larger estimation errors resulting in less accurate model updating parameters. To study the effect of modeling errors, two modeling error cases are considered, one with error in underlying linear model and the other with error in local nonlinearity. The results verify that Bayesian approach has the capability of providing parameters estimation uncertainties and selecting the more suitable model class based on the measured data.

Acknowledgements

Partial support of this study by the National Science Foundation Grant number 1254338 is gratefully acknowledged. L. Renson was partly funded by the European Union's Horizon 2020 research and innovation programme under the Marie Sklodowska-Curie grant agreement No. 703204, and by the Royal Academy of Engineering (research fellowship RF1516/15/11). J.P. Noël is a Postdoctoral Researcher of the "Fonds de la Recherche Scientifique – FNRS" which is gratefully acknowledged. The opinions, findings, and conclusions expressed in this paper are those of the authors and do not necessarily represent the views of the sponsors and organizations involved in this project.

Reference

1. Zienkiewicz OC, Taylor RL and Taylor RL. *The finite element method*. McGraw-hill London, 1977.
2. Mottershead J and Friswell M. Model updating in structural dynamics: a survey. *Journal of sound and vibration* 1993; 167: 347-75.
3. Friswell M and Mottershead JE. *Finite element model updating in structural dynamics*. Springer Science & Business Media, 2013.
4. Brownjohn JM and Xia P-Q. Dynamic assessment of curved cable-stayed bridge by model updating. *Journal of Structural Engineering* 2000; 126: 252-60.
5. Teughels A and De Roeck G. Structural damage identification of the highway bridge Z24 by FE model updating. *Journal of Sound and Vibration* 2004; 278: 589-610.
6. Reynders E, Roeck GD, Gundes Bakir P and Sauvage C. Damage identification on the Tilff bridge by vibration monitoring using optical fiber strain sensors. *Journal of engineering mechanics* 2007; 133: 185-93.
7. Song M, Yousefianmoghadam S, Mohammadi M-e, Moaveni B, Stavridis A and Wood RL. An application of FE model updating for damage assessment of a full scale two-story RC building and comparison with lidar measurements. *Structural health monitoring* 2017, accepted.
8. Asgarieh E, Moaveni B and Stavridis A. Nonlinear finite element model updating of an infilled frame based on identified time-varying modal parameters during an earthquake. *Journal of Sound and Vibration* 2014; 333: 6057-73.

9. Asgarieh E, Moaveni B, Barbosa AR and Chatzi E. Nonlinear model calibration of a shear wall building using time and frequency data features. *Mechanical Systems and Signal Processing* 2017; 85: 236-51.
10. Kyprianou A, Worden K and Panet M. Identification of hysteretic systems using the differential evolution algorithm. *Journal of Sound and Vibration* 2001; 248: 289-314.
11. Schmidt R. Updating non-linear components. *Mechanical Systems and Signal Processing* 1994; 8: 679-90.
12. Doebling S, Hemez F and Rhee W. Statistical model updating and validation applied to nonlinear transient structural dynamics. *Proceedings of the European COST F3 Conference on System Identification & Structural Health Monitoring, Madrid*. Citeseer, 2000, p. 409-18.
13. Schultze JF, Hemez FM, Doebling SW and Sohn H. Application of non-linear system model updating using feature extraction and parameter effects analysis. *Shock and Vibration* 2001; 8: 325-37.
14. Hemez FM and Doebling SW. Review and assessment of model updating for non-linear, transient dynamics. *Mechanical Systems and Signal Processing* 2001; 15: 45-74.
15. Meyer S and Link M. Modelling and updating of local non-linearities using frequency response residuals. *Mechanical Systems and Signal Processing* 2003; 17: 219-26.
16. Kerschen G and Golinval J-C. Generation of accurate finite element models of nonlinear systems–application to an aeroplane-like structure. *Nonlinear Dynamics* 2005; 39: 129-42.
17. Kurt M, Eriten M, McFarland DM, Bergman LA and Vakakis AF. Methodology for model updating of mechanical components with local nonlinearities. *Journal of Sound and Vibration* 2015; 357: 331-48.
18. Kurt M, Moore KJ, Eriten M, McFarland DM, Bergman LA and Vakakis AF. Nonlinear model updating applied to the IMAC XXXII Round Robin benchmark system. *Mechanical Systems and Signal Processing* 2017; 88: 111-22.
19. Alampalli S. Effects of testing, analysis, damage, and environment on modal parameters. *Mechanical Systems and Signal Processing* 2000; 14: 63-74.
20. Clinton JF, Bradford SC, Heaton TH and Favela J. The observed wander of the natural frequencies in a structure. *Bulletin of the Seismological Society of America* 2006; 96: 237-57.
21. Sohn H. A Bayesian probabilistic approach for structure damage detection. 1997:
22. Beck JL and Katafygiotis LS. Updating models and their uncertainties. I: Bayesian statistical framework. *Journal of Engineering Mechanics* 1998; 124: 455-61.
23. Beck JL, Au SK and Vanik MW. Monitoring structural health using a probabilistic measure. *Computer‐Aided Civil and Infrastructure Engineering* 2001; 16: 1-11.
24. Beck JL and Au S-K. Bayesian updating of structural models and reliability using Markov chain Monte Carlo simulation. *Journal of Engineering Mechanics* 2002; 128: 380-91.
25. Beck JL. Bayesian system identification based on probability logic. *Structural Control and Health Monitoring* 2010; 17: 825-47.
26. Ching J and Beck JL. New Bayesian model updating algorithm applied to a structural health monitoring benchmark. *Structural Health Monitoring* 2004; 3: 313-32.
27. Yuen KV, Beck JL and Au SK. Structural damage detection and assessment by adaptive Markov chain Monte Carlo simulation. *Structural Control and Health Monitoring* 2004; 11: 327-47.
28. Muto M and Beck JL. Bayesian updating and model class selection for hysteretic structural models using stochastic simulation. *Journal of Vibration and Control* 2008; 14: 7-34.

29. Ntotsios E, Papadimitriou C, Panetsos P, Karaiskos G, Perros K and Perdikaris PC. Bridge health monitoring system based on vibration measurements. *Bulletin of Earthquake Engineering* 2009; 7: 469.
30. Behmanesh I, Moaveni B and Papadimitriou C. Probabilistic damage identification of a designed 9-story building using modal data in the presence of modeling errors. *Engineering Structures* 2017; 131: 542-52.
31. Behmanesh I, Moaveni B, Lombaert G and Papadimitriou C. Hierarchical Bayesian model updating for structural identification. *Mechanical Systems and Signal Processing* 2015; 64: 360-76.
32. Rosenberg R. The normal modes of nonlinear n-degree-of-freedom systems. *Journal of applied Mechanics* 1962; 29: 7-14.
33. Rosenberg R. On nonlinear vibrations of systems with many degrees of freedom. *Advances in applied mechanics* 1966; 9: 155-242.
34. Lee YS, Kerschen G, Vakakis AF, Panagopoulos P, Bergman L and McFarland DM. Complicated dynamics of a linear oscillator with a light, essentially nonlinear attachment. *Physica D: Nonlinear Phenomena* 2005; 204: 41-69.
35. Shaw SW and Pierre C. Normal modes for non-linear vibratory systems. *Journal of sound and vibration* 1993; 164: 85-124.
36. Vakakis AF, Manevitch LI, Mikhlin YV, Pilipchuk VN and Zevin AA. *Normal modes and localization in nonlinear systems*. Springer, 2001.
37. Vakakis AF. Non-linear normal modes (NNMs) and their applications in vibration theory: an overview. *Mechanical systems and signal processing* 1997; 11: 3-22.
38. Kuether RJ, Renson L, Detroux T, Grappasonni C, Kerschen G and Allen MS. Nonlinear normal modes, modal interactions and isolated resonance curves. *Journal of Sound and Vibration* 2015; 351: 299-310.
39. Renson L, Noël J-P and Kerschen G. Complex dynamics of a nonlinear aerospace structure: numerical continuation and normal modes. *Nonlinear Dynamics* 2015; 79: 1293-309.
40. Peter S, Grundler A, Reuss P, Gaul L and Leine RI. Towards finite element model updating based on nonlinear normal modes. *Nonlinear Dynamics, Volume 1*. Springer, 2016, p. 209-17.
41. Hill T, Green P, Cammarano A and Neild S. Fast Bayesian identification of a class of elastic weakly nonlinear systems using backbone curves. *Journal of Sound and Vibration* 2016; 360: 156-70.
42. Peeters M, Kerschen G and Golinval J-C. Modal testing of nonlinear vibrating structures based on nonlinear normal modes: experimental demonstration. *Mechanical Systems and Signal Processing* 2011; 25: 1227-47.
43. Renson L, Gonzalez-Buelga A, Barton D and Neild S. Robust identification of backbone curves using control-based continuation. *Journal of Sound and Vibration* 2016; 367: 145-58.
44. Peter S and Leine RI. Excitation power quantities in phase resonance testing of nonlinear systems with phase-locked-loop excitation. *Mechanical Systems and Signal Processing* 2017; 96: 139-58.
45. Noël J-P, Renson L, Grappasonni C and Kerschen G. Identification of nonlinear normal modes of engineering structures under broadband forcing. *Mechanical Systems and Signal Processing* 2016; 74: 95-110.

46. Peeters M, Viguié R, Sérandour G, Kerschen G and Golinval J-C. Nonlinear normal modes, Part II: Toward a practical computation using numerical continuation techniques. *Mechanical systems and signal processing* 2009; 23: 195-216.
47. Jaynes ET. Information theory and statistical mechanics. *Physical review* 1957; 106: 620.
48. Jaynes ET. Information theory and statistical mechanics. II. *Physical review* 1957; 108: 171.
49. Renson L, Kerschen G and Cochelin B. Numerical computation of nonlinear normal modes in mechanical engineering. *Journal of Sound and Vibration* 2016; 364: 177-206.
50. Simoen E, Moaveni B, Conte JP and Lombaert G. Uncertainty quantification in the assessment of progressive damage in a 7-story full-scale building slice. *Journal of Engineering Mechanics* 2013; 139: 1818-30.
51. Thouverez F. Presentation of the ECL benchmark. *Mechanical Systems and Signal Processing* 2003; 17: 195-202.
52. Grappasonni C, Noël J-P and Kerschen G. Subspace and nonlinear-normal-modes-based identification of a beam with softening-hardening behaviour. *Nonlinear Dynamics, Volume 2*. Springer, 2014, p. 55-68.
53. MATLAB R2014a. In: MathWorks, (ed.). 2014.
54. Byrd RH, Hribar ME and Nocedal J. An interior point algorithm for large-scale nonlinear programming. *SIAM Journal on Optimization* 1999; 9: 877-900.
55. Metropolis N, Rosenbluth AW, Rosenbluth MN, Teller AH and Teller E. Equation of state calculations by fast computing machines. *The journal of chemical physics* 1953; 21: 1087-92.
56. Hastings WK. Monte Carlo sampling methods using Markov chains and their applications. *Biometrika* 1970; 57: 97-109.
57. Roberts GO and Rosenthal JS. Optimal scaling for various Metropolis-Hastings algorithms. *Statistical science* 2001; 16: 351-67.
58. Ching J and Chen Y-C. Transitional Markov chain Monte Carlo method for Bayesian model updating, model class selection, and model averaging. *Journal of engineering mechanics* 2007; 133: 816-32.
59. Betz W, Papaioannou I and Straub D. Transitional markov chain monte carlo: observations and improvements. *Journal of Engineering Mechanics* 2016; 142: 04016016.
60. Wu S, Angelikopoulos P, Papadimitriou C and Koumoutsakos P. Bayesian Annealed Sequential Importance Sampling: An Unbiased Version of Transitional Markov Chain Monte Carlo. *ASCE-ASME Journal of Risk and Uncertainty in Engineering Systems, Part B: Mechanical Engineering* 2018; 4: 011008.